Research Article | Vol. 24, No. 16 | 8 Aug 2016 | OPTICS EXPRESS 17553

Optics EXPRESS

Manganese-doped near-infrared emitting nanocrystals for *in vivo* biomedical imaging

WING-CHEUNG LAW,[1,2,*] ZHOURUI XU,[2] KEN-TYE YONG,[3] XIN LIU,[4] MARK T. SWIHART,[4] MUKUND SESHADRI,[5] AND PARAS N. PRASAD[1,6]

[1]*Institute for Lasers, Photonics, and Biophotonics, University at Buffalo, Buffalo, New York, USA*
[2]*Department of Industrial and Systems Engineering, The Hong Kong Polytechnic University, Hung Hom, Kowloon, Hong Kong, China*
[3]*School of Electrical and Electronic Engineering, Nanyang Technological University, Singapore 639798, Singapore.*
[4]*Department of Chemical and Biological Engineering, University at Buffalo, Buffalo, New York, USA*
[5]*Department of Pharmacology and Therapeutics, Roswell Park Cancer Institute, Buffalo, New York, USA*
[6]*pnprasad@buffalo.edu*
[*]*roy.law@polyu.edu.hk*

Abstract: Nanoprobes with multiple imaging modality have attracted a great deal of attention due to the capability of offering complementary information from each individual component. This work presents a hybrid approach to synthesize manganese doped near infrared (NIR) emitting quantum dots. The Mn-doping process was accomplished in aqueous phase followed by a phase transfer to organic phase for ZnS coating. This bimodal nanoprobe displayed high NIR luminescence quantum yield (~14%) and capability of magnetic resonance imaging (MRI) (1.44 mM^{-1} s^{-1}). The RGD-targeted nanoprobes have been exploited for *in vitro* cell labelling, *in vivo* tumor targeting and lymph node mapping. In addition, no adverse toxic effects were observed, demonstrating the high biocompatibility of this nanoprobe.

OCIS codes: (160.0160) Materials; (160.4236) Nanomaterials.

References and links

1. P. N. Prasad, *Introduction to Nanomedicine and Nanobioengineering* (Wiley-Interscience, 2013).
2. S. Kim, Y. T. Lim, E. G. Soltesz, A. M. De Grand, J. Lee, A. Nakayama, J. A. Parker, T. Mihaljevic, R. G. Laurence, D. M. Dor, L. H. Cohn, M. G. Bawendi, and J. V. Frangioni, "Near-infrared fluorescent type II quantum dots for sentinel lymph node mapping," Nat. Biotechnol. **22**(1), 93–97 (2004).
3. G. J. Stasiuk, S. Tamang, D. Imbert, C. Poillot, M. Giardiello, C. Tisseyre, E. L. Barbier, P. H. Fries, M. de Waard, P. Reiss, and M. Mazzanti, "Cell-permeable Ln(III) chelate-functionalized InP quantum dots as multimodal imaging agents," ACS Nano **5**(10), 8193–8201 (2011).
4. A. Becker, C. Hessenius, K. Licha, B. Ebert, U. Sukowski, W. Semmler, B. Wiedenmann, and C. Grötzinger, "Receptor-targeted optical imaging of tumors with near-infrared fluorescent ligands," Nat. Biotechnol. **19**(4), 327–331 (2001).
5. X. Liu, C. Lee, W.-C. Law, D. Zhu, M. Liu, M. Jeon, J. Kim, P. N. Prasad, C. Kim, and M. T. Swihart, "Au-Cu_{2-x}Se heterodimer nanoparticles with broad localized surface plasmon resonance as contrast agents for deep tissue imaging," Nano Lett. **13**(9), 4333–4339 (2013).
6. B. E. Rolfe, I. Blakey, O. Squires, H. Peng, N. R. B. Boase, C. Alexander, P. G. Parsons, G. M. Boyle, A. K. Whittaker, and K. J. Thurecht, "Multimodal polymer nanoparticles with combined 19f magnetic resonance and optical detection for tunable, targeted, multimodal imaging in vivo," J. Am. Chem. Soc. **136**(6), 2413–2419 (2014).
7. Q. Xiao, X. Zheng, W. Bu, W. Ge, S. Zhang, F. Chen, H. Xing, Q. Ren, W. Fan, K. Zhao, Y. Hua, and J. Shi, "A core/satellite multifunctional nanotheranostic for in vivo imaging and tumor eradication by radiation/photothermal synergistic therapy," J. Am. Chem. Soc. **135**(35), 13041–13048 (2013).
8. L. Liu, W. C. Law, K. T. Yong, I. Roy, H. Ding, F. Erogbogbo, X. Zhang, and P. N. Prasad, "Multimodal imaging probes based on Gd-DOTA conjugated quantum dot nanomicelles," Analyst (Lond.) **136**(9), 1881–1886 (2011).
9. K.-T. Yong, "Mn-doped near-infrared quantum dots as multimodal targeted probes for pancreatic cancer imaging," Nanotechnology **20**(1), 015102 (2009).
10. S. K. Panda, S. G. Hickey, H. V. Demir, and A. Eychmüller, "Bright white-light emitting manganese and copper co-doped ZnSe quantum dots," Angew. Chem. Int. Ed. Engl. **50**(19), 4432–4436 (2011).

#265250 http://dx.doi.org/10.1364/OE.24.017553
Journal © 2016 Received 16 May 2016; revised 16 Jul 2016; accepted 18 Jul 2016; published 25 Jul 2016

Optics EXPRESS

11. G. Chen, T. Y. Ohulchanskyy, S. Liu, W. C. Law, F. Wu, M. T. Swihart, H. Agren, and P. N. Prasad, "Core/shell $NaGdF_4$:Nd^{3+}/$NaGdF_4$ nanocrystals with efficient near-infrared to near-infrared downconversion photoluminescence for bioimaging applications," ACS Nano **6**(4), 2969–2977 (2012).
12. L. M. Maestro, E. M. Rodriguez, F. Vetrone, R. Naccache, H. L. Ramirez, D. Jaque, J. A. Capobianco, and J. G. Solé, "Nanoparticles for highly efficient multiphoton fluorescence bioimaging," Opt. Express **18**(23), 23544–23553 (2010).
13. T. Jin and Y. Imamura, "Applications of highly bright pbs quantum dots to non-invasive near-infrared fluorescence imaging in the second optical window," ECS J. Solid State Sci. Technol. **5**(1), R3138–R3145 (2016).
14. G. Sitbon, S. Bouccara, M. Tasso, A. Francois, L. Bezdetnaya, F. Marchal, M. Beaumont, and T. Pons, "Multimodal Mn-doped I-III-VI quantum dots for near infrared fluorescence and magnetic resonance imaging: from synthesis to in vivo application," Nanoscale **6**(15), 9264–9272 (2014).
15. L. Turyanska, F. Moro, A. N. Knott, M. W. Fay, T. D. Bradshaw, and A. Patanè, "Paramagnetic, near-infrared fluorescent mn-doped pbs colloidal nanocrystals," Part. Part. Syst. Charact. **30**(11), 945–949 (2013).
16. W.-C. Law, K.-T. Yong, I. Roy, H. Ding, R. Hu, W. Zhao, and P. N. Prasad, "Aqueous-phase synthesis of highly luminescent cdte/znte core/shell quantum dots optimized for targeted bioimaging," Small **5**(11), 1302–1310 (2009).
17. L. J. Sang and H. F. Wang, "Aminophenylboronic-acid-conjugated polyacrylic acid-Mn-doped ZnS quantum dot for highly sensitive discrimination of glycoproteins," Anal. Chem. **86**(12), 5706–5712 (2014).
18. L. Damalakiene, V. Karabanovas, S. Bagdonas, M. Valius, and R. Rotomskis, "Intracellular distribution of nontargeted quantum dots after natural uptake and microinjection," Int. J. Nanomedicine **8**(10), 555–568 (2013).
19. L. Ye, K.-T. Yong, L. Liu, I. Roy, R. Hu, J. Zhu, H. Cai, W.-C. Law, J. Liu, K. Wang, J. Liu, Y. Liu, Y. Hu, X. Zhang, M. T. Swihart, and P. N. Prasad, "A pilot study in non-human primates shows no adverse response to intravenous injection of quantum dots," Nat. Nanotechnol. **7**(7), 453–458 (2012).
20. J. Liu, W.-C. Law, J. Liu, R. Hu, L. Liu, J. Zhu, H. Chen, J. Wang, Y. Hu, L. Ye, and K.-T. Yong, "Toxicity assessment of phospholipid micelle-encapsulated cadmium-based quantum dots using Kunming mice," RSC Advances **3**(6), 1768–1773 (2013).

1. Introduction

Biomodal nanoprobes have emerged as powerful materials for nano-theranostics applications [1]. One of the important reasons is that nanoprobes with multiple imaging modalities can offer complementary information from each individual component and hence overcome the limitations from the single-modality counterparts. For instance, as demonstrated by research groups, fluorescence imaging could provide optical guidance to surgeons for precisely removing infectious regions [2] while the MRI could offer high spatial resolution and the capability of 3-dimension image reconstruction for whole body imaging [3], thus makes optical-magnetic incorporated nanoprobes highly desirable. In addition, the use of near infrared (NIR, 700 – 1100 nm) emitting quantum dots (QDs) could enhance the signal-to-noise ratio in optical imaging. It is because the autofluorescence and scattering by the biological tissues are minimum within this NIR region, or so-called biological transparent window, thus the use of NIR light source would allow us to have deep tissue examinations [4, 5]. However, the poor spatial resolution of optical imaging was still the major obstacle for widely use. To address this issue, a various type of nanoprobes with multiple imaging modalities, that integrated the strengths of each individual imaging modality into one system, has been developed [6, 7]. By correlating the images/data obtained in different modalities, the accuracy and speed of diagnosis can be increased.

Among various types of multimodal nanoprobes, the integration of optical and magnetic imaging modalities has attracted most attention because this combination can provide complementary solution. In particular, our group demonstrated a dual modal imaging in head and neck tumor studies utilizing a Gd^{3+} containing nanoformulation including NIR-emitting fluorophores [8]. Another powerful approach for producing multimodal nanoprobes was ion doping [9]. Unlike the chelation and the co-encapsulation approaches, doping is usually carried out during the synthesis. It does not require any post-treatment of the as-prepared nanoparitcles for the addition of modalities and thus the particle size will not be affected. Doping is a widely used technique for tuning the optical properties of nanoparticles. For example, the emission of doped QDs can be tuned by controlling the dopant concentrations [10]. Another typical example is the upconversion nanoparticles in which the upconverting

Optics EXPRESS

process can be tailored by the lanthanide ions doped in a ceramic matrix [11, 12]. Several reports related to the preparation of manganese (Mn) doped QDs were found [13–15].Sitbon et. al. synthesized multimodal QDs by doping Mn in the thick ZnS shells [14].Turyanska et. al. and Takashi et. al. incorporated the paramagnetism into NIR QDs using Mn doped PbS [13, 15]. Most of the doping processes were carried out in organic synthetic route which enabled us to have high quality and stable nanoparticles. However, expensive chemicals, high operating temperature, toxic solvents (e.g. pyrophoric acid) and air-free condition are also required and they have become the drawbacks of this synthetic approach. In comparison, direct aqueous synthesis can be exploited as powerful alternative for synthesizing high quality QD with less demand to the critical environments. Our previous study demonstrated a one-pot aqueous synthesis of CdTe/ZnTe QD optimized for bioimaging [16]. However, the preparation of doped-QDs directly in aqueous phase and used for bimodal imaging were seldom reported [17]. In this contribution, a hybrid approach was employed to synthesize ZnS coated Mn-doped NIR emitting QDs (Mn:NIR-QDs) for *in vivo* bioimaging including tumor targeting and sentinel lymph node mapping. Mn:NIR-QDs were firstly synthesized in aqueous phase then transferred to organic phase to ensure the complete removal of free ion (e.g. Mn^{2+}, Hg^{2+}). The organic phase Mn:NIR-QDs were systemically characterized and exhibited both excellent NIR luminescence and MRI contrast without any free ion interference. Mn:NIR-QDs were then passivated with phospholipid to functionalize the nanoprobes, enhancing the biocompatibility and prolong the circulation time *in vivo*. The toxicity assessments were also performed *in vitro* and *in vivo* and no adverse effects were found, indicating the promise of using these bimodal nanoprobes for *in vivo* cancer detection.

2. Results and discussion

2.1. Mn:NIR-QD synthesis and characterizations

Briefly, 128 mg of tellurium powder and 80 mg of sodium borohydride were mixed with 5 mL of degassed water. The mixture was stirred for 2-3 hours until a light-pink solution was observed. We refer this solution as the Te precursor. Next, 2 mmol of $Cd(ClO_4)_2$, 5 mmol of cysteine, and 150 mL of water were mixed into a three-necked flask under stirring. The pH was adjusted to 9.5 by adding sodium hydroxide solution. The flask was sealed and 1.5 mL of Te precursor was injected quickly into the mixture under nitrogen. Hg-precursor was prepared by dissolving 0.2-0.3 mmol of $Hg(ClO_4)_2$, 0.5 mmol of cysteine into water with pH 9.5. The Hg-precursor was injected to the CdTe solution at room temperature dropwise. The color of solution changed from dark red to black upon the injection. The reaction mixture was slowly heated to 100 °C. After 30 minutes, Mn-precursor was prepared by dissolving 0.24 mmol of $Mn(ClO_4)_2$, 0.3 mmol of cysteine into water and injected dropwise to the hot reaction solution. At the desire emission wavelength, the quantum dots were purified from the surfactant solution by the addition of ethanol and centrifugation. The aqueous synthesized QDs were transferred to organic phase using dodecanethiol. Briefly, purified QDs were dispersed into 5 mL of water, then a mixture of 5 mL of dodecanethiol, 5 mL of butanol and 2 mL of acetone was added. After stirring for 2 minutes, 200 µl of NH_4OH was added. The transferred QDs were purified and re-dispersed in chloroform by the addition of ethanol and centrifugation. For ZnS shell coating, a solution containing 5 g of trioctylphosphine oxide, 5 mL of oleic acid and 2 mmol of zinc acetate were prepared and heated to 100 °C under nitrogen until a clear solution was observed. The Mn:CdHgTe core solution was injected slowly under stirring into the hot reaction mixture with a needle outlet that allowed the chloroform to evaporate. The temperature was then raised to 170-180 °C. Upon reaching the desired temperature, 1 mL of 1 mM TOP-S solution (32 mg of sulfur dissolved in 1 mL of TOP) was added dropwise into the reaction mixture. The mixture was then maintained at ~180 °C for 2-3 minutes and then separated by addition of ethanol and centrifugation. The as-prepared Mn:NIR-QDs were filtered with PTFE syringe filter (0.45 µm pore size) and then dried using the evaporator. The dried film was redispersed in chloroform at a concentration of

Optics EXPRESS

2 mgmL^{-1}. 0.2 mL of Mn:NIR-QD suspension was mixed with chloroform solutions of DSPE–mPEG-2000, mPEG-NH2 and DSPE–PEG–Mal at a weight ratio of 4:1:1 (4mg:1mg:1mg) in around bottomed flask with gentle stirring for 5 minutes. Chloroform was then evaporated using a rotary vacuum evaporator. After evaporation, the residue film was heated to 50-60 °C and HPLC-grade water was added. The nanomicelle suspension was filtered through a 0.2 μm filter and purified by centrifugation at 11000 rpm for 15 minutes. The supernatant was removed and the nanomicelles were redispersed in HPLC water. Maleimide-terminated nanomicelles were mixed with excess cyclic-RGD peptide in PBS solution (pH = 7.2) for bioconjugation. After 2 hours of incubation, the mixture was centrifuged at 11000 rpm for 15 minutes to remove excess cyclic-RGD peptide and redispersed in 200 μL of PBS (the concentration was referred as 2 mgmL^{-1}). Nanomicelles without RGD peptide conjugation were used in the control experiment.

Figure 1(a) shows the TEM image of Mn:NIR-QDs dispersed in organic solvent. The lattice fringes are readily shown in the inset. The size of the particle was estimated as 3.3 nm in diameter. TEM image of phospholipid encapsulated Mn:NIR-QDs dispersed in aqueous media is shown in Fig. 1(b). A closely packed QD micelle is illustrated with approximately 60 – 70 nm in diameter. It is worth mentioning that the hydrohynamic diameter of Mn:NIR-QDs was ~120nm measured by a dynamic light scattering machine. This is because the polymeric shell was not detectable in TEM. The dispersion of aqueous QD was clear and no precipitation was observed. To examine the crystal structure of Mn:NIR-QDs, x-ray diffraction (XRD) profile of Mn:NIR-QDs is shown in Fig. 1(c). The strong peaks at the 2θ values 25.1∘, 41.7∘ and 48.3∘show that the Mn:NIR-QDs have zinc blende structure. Furthermore, the elemental composition of Mn:NIR-QDs were analyzed using energy-dispersive X-ray (EDX) spectroscopy. Part d of Fig. 1 confirms the presence of Cd, Hg, Te and Mn elements. On the basis of the proportion of Hg and Mn measured from the EDX (Hg:6.1%, Mn: 5.7%), we assigned the ratio $Cd_{0.64}Hg_{0.06}Mn_{0.06}Te_{0.24}$.

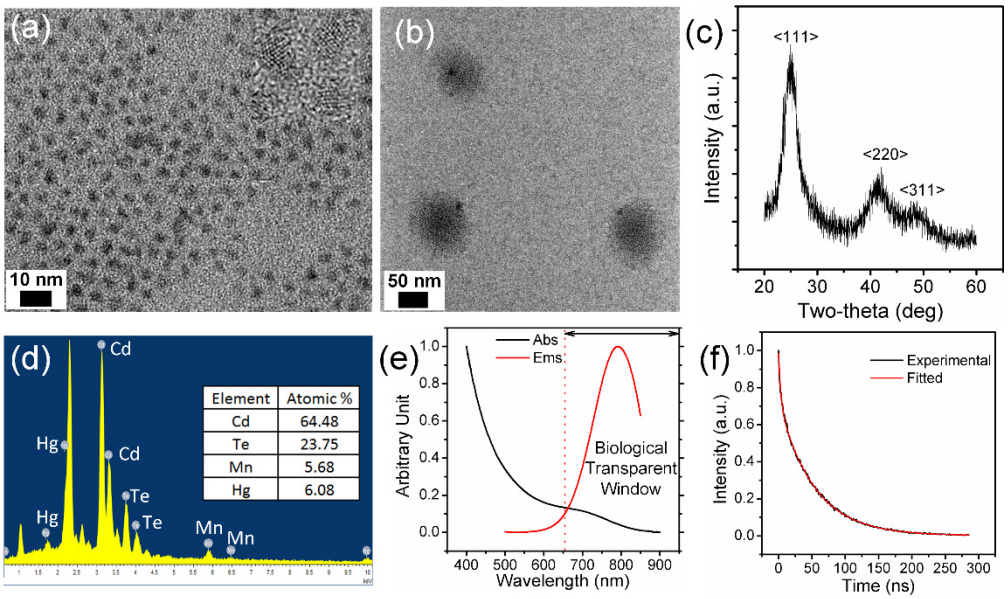

Fig. 1. TEM image of Mn:NIR-QDs dispersed in (a) organic solvent and (b) aqueous media. (c) XRD, (d) EDX, (e) absorption, emission (excitation: 488nm) and (f) lifetime (excitation: 650nm) profile of Mn:NIR-QDs.

The luminescence and absorption spectra of micelle-encapsulated Mn:NIR-QDs are shown in Fig. 1(e). The emission peak of this ternary-cored QD is ~791nm which lies into the so-called “biological transparent window”. Emission in this region is an excellent nanoprobe

Optics EXPRESS

for *in vivo* biological imaging because of the minimal absorption by the biological tissues [1] thus enabling a deeper penetration through the tissue and an easy signal subtraction from the autofluorescence background. The quantum yield of Mn:NIR-QD is estimated ~14% measured according to the typical procedures using Cy5.5 as a reference. Both Mn:NIR-QD and Cy5.5 were diluted to have same absorbance (~0.3) at 680nm. The QY was determined by comparing the integration under the emission curves. The time-resolved PL of Mn:NIR-QD has been studied by an EasyLife LS fluorescence lifetime system (Photon Technology International, Inc., Lawrenceville, NJ) with an excitation source 650nm. An exponential decay is shown in Fig. 1 (f). The measured decay curve (black) was fitted by a single-exponential formula (red) as given below:

$$y = \exp\left(-t/\tau\right)$$

where τ is the decay time constant. In this case, the decay lifetime was estimated ~52 ns. Comparing with the organic compounds, which the typical fluorescence lifetime is in ns, the longer decay time of Mn:NIR-QD can be potentially served as contrast agent in time-resolved microscopy because it can be easily detected by fluorescence lifetime imaging microscopy (FLIM).

The magnetic behavior of Mn:NIR-QDs were analyzed using vibrating sample magnetometer (VSM). From the hysteresis loops as shown in Fig. 2 (a), which is associated with the Mn^{2+}, the Mn:NIR-QD can be categorized as paramagnetic material. This paramagnetic property was further characterized to evaluate the capability of serving as a magnetic resonance imaging (MRI) contrast agent. The efficacy of Mn^{2+} as T1 (the longitudinal proton relaxation time) contrast was assessed by a MR relaxometry (General Electric 4.7 T/33 cm horizontal bore magnet (GE NMRinstruments, Fremont, CA) incorporating AVANCE digital electronics (Bruker BioSpec platform with ParaVision Version 3.0.2 acquisition software, Bruker Medical, Billerica, MA)). The relaxation rate R_1 ($1/T_1$) at different concentrations of Mn:NIR-QDs were measured, and plotted against the concentration, as shown in Fig. 2 (b). The relaxivity (r_1) of Mn:NIR-QD was determined from the slope of the linear plot and 1.44 mM^{-1} s^{-1} was obtained, indicating the magnetic modality of Mn:NIR-QD.

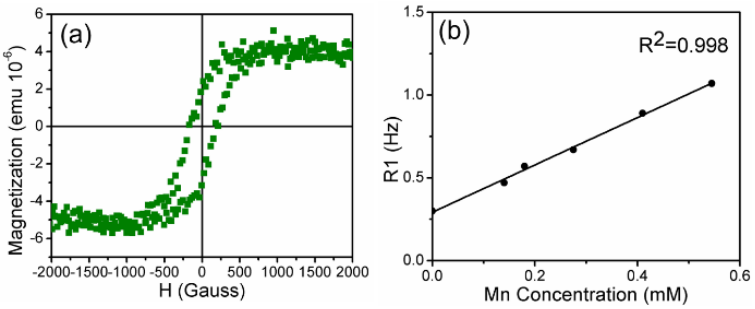

Fig. 2. (a) Hysteresis curve of Mn:NIR-QDs obtained at room temperature (25°C); (b) R_1 relaxivity of Mn:NIR-QD nanomicelles in water.

2.2. In vitro cell labelling and cytotoxicity

For *in vitro* studies, RAW264.7 macrophage cell lines were treated with Mn:NIR-QDs in a 6-well plate with culture medium (Dulbecco's Modified Eagle Medium, DMEM). One day before the treatment, cells were seeded on cover glass slips. Then the glass slips with ~50-60% confluency were treated with phospholipid encapsulated Mn:NIR-QD at a final concentration of 100 μg/mL. After 2 hours, dishes were rinsed three times with DMEM and imaged using Nuance™ optical microscopy complied with "Deep Red" filter set (Objective: 63x, excitation: 661nm, emission: 700 nm long pass). As demonstrated in Fig. 3, a robust NIR

Optics EXPRESS

signal, which was originated from the Mn:NIR-QD, was clearly observed from the cells. The cellular uptake was not obvious because these nonfunctionalized QDs were passively uptaken by the macrophages via endocytosis [18].

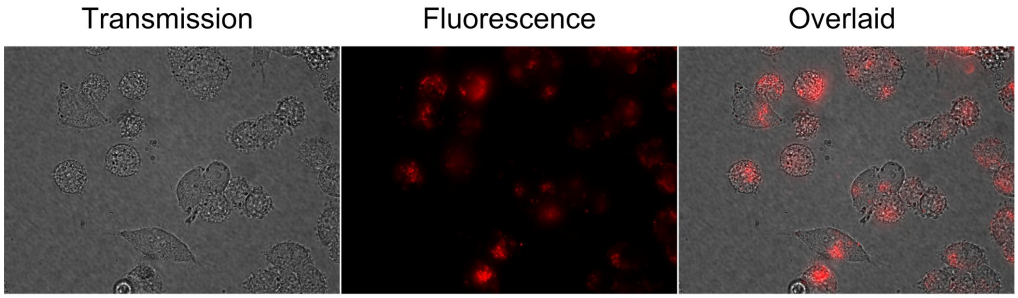

Fig. 3. Cell images of macrophages treated with NIR-emitting Mn:NIR-QDs.

Although a tremendous success of utilizing QDs for biomedical applications has been witnessed, a lot toxicity issues have also been raised. Many studies suggested that the impact of the heavy-metal containing candidates to human health is still unclear which may be detrimental to their clinical utility. Recently, heavy-metal containing materials have been tested in non-human primates over 90 days. No evidence of toxicity was shown in the phospholipid micelle encapsulated Cd-based QDs [19]. It implicated that the toxicity of heavy-metals can be drastically reduced or precluded when their integrities can be maintained. To investigate the potential toxicity of Mn:NIR-QDs towards the biological subjects, *in vitro* and *in vivo* assessments have been performed. Before administrating the Mn:NIR-QD to the animals, the potential cytotoxicity was assessed by MTS assay on Panc-1 cell line. Figure 4 depicts the viability result of Panc-1 cells treated with various concentration of Mn:NIR-QDs for 24 and 48 hours. Even at high concentration (500μg/mL), the cell viability can be maintained over 65%, indicating the high biocompatibility of Mn:NIR-QD at the safe dosages.

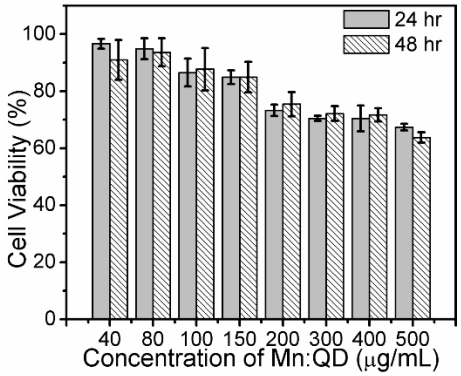

Fig. 4. Cytotoxicity studies of cells treated with the Mn:NIR-QDs. MTS assays illustrating percentage cell viability (compared to nontreated cells being arbitrarily assigned 100% viability) upon exposing the cells to different concentrations of Mn:NIR-QD nanomicelles for 24 and 48 hours.

2.3. In vivo tumor targeting and sentinel lymph node (SLN) mapping

To demonstrate the *in vivo* tumor targeting capability, Mn:NIR-QDs were functionalized with RGD peptide (RGD-Mn:NIR-QD) through the thiol-maleimide linkage. It is worth mentioning that the RGD peptide specifically targeted the $\alpha_v\beta_3$ integrin receptors which are overexpressed on the tumor. Nude mice bearing Panc-1 subcutaneous xenograft were intravenously injected with RGD-Mn:NIR-QD (25mg/kg). Live whole body imaging was

Optics EXPRESS

performed at various time points (3, 6, 20 and 24 hr) post injection using the Maestro *in vivo* imaging system (CRI, Inc). As shown in Fig. 5, the luminescence intensity of Mn:NIR-QD accumulated at the tumor site and reached the maximum at 20 hr post injection (Excitation: 635nm, emission: 675nm long pass, integration time: 1500ms). In sharp contrast, for the control mice intravenously injected with Mn:NIR-QD without RGD functionalization, minimal luminescence signal was observed at the tumor site. This demonstrated the tumor specificity of Mn:NIR-QD was facilitated by the RGD peptide.

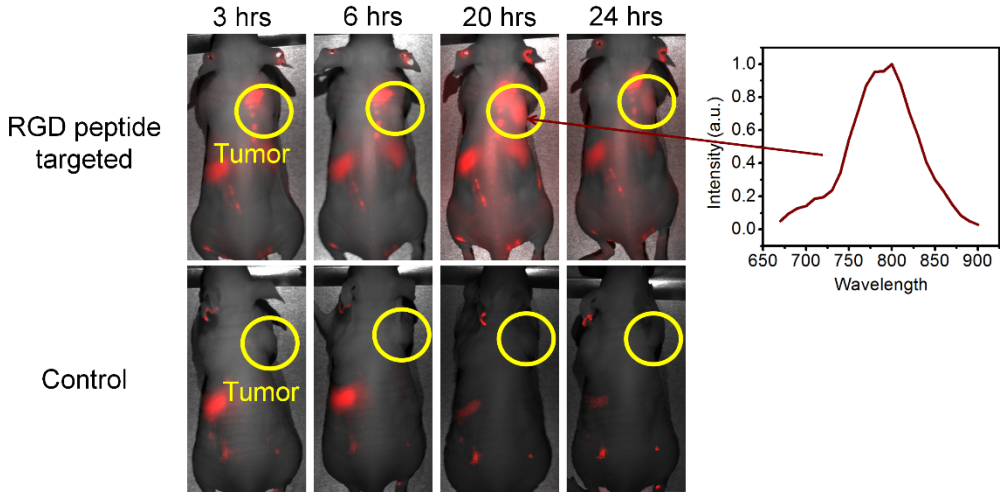

Fig. 5. Time-dependent *in vivo* imaging of Panc-1 tumor bearing mice (right shoulder, indicated by yellow arrow) treated with RGD-conjugated (upper panel) and unconjugated (lower panel) Mn:NIR-QD nanomicelles. All images were acquired under the same conditions. Inset is the luminescence spectrum of Mn:NIR-QD.

To confirm the superior accumulation of RGD-Mn:NIR-QD in the tumor, ex vivo imaging was performed after sacrificing the mice at 24 hr post injection. Major organs (liver, spleen, kidney, heart and lung) and tumor were resected and imaged under the same condition. As shown in Fig. 6(a), strong QD signals are detected in lung and spleen in both case due to the capture by the reticuloendothelial system (RES). It is noted that for the control group treated with PEGylated Mn:NIR-QD, minimal QD signal was observed as compared with the strong signal obtained in RGD-Mn:NIR-QD treated group, which shows good agreement with data shown in Fig. 5.

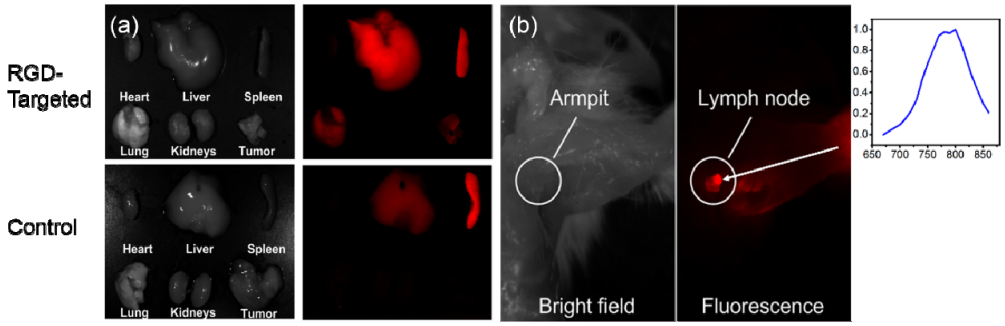

Fig. 6. (a) Luminescence images of major organs and tumors harvested at 24 hr post injection. (b) SLN imaging at 45 minutes post injection of Mn:NIR-QD into left paw. Inset is the luminescence spectrum of Mn:NIR-QD.

NIR imaging is of great importance for biomedical research. It is not only suitable for deep tissue imaging due to the penetration power of NIR emission but also served as assisting

Optics EXPRESS

tool for surgeon to precisely remove the infected tissue as it doesn't interfere with the visible light. For example, sentinel lymph node (SLN) is a major pathway of spread of cancer. Therefore, lymph node mapping or removal are valuable for diagnosis or treatment of the metastatic stage of cancer. To demonstrate the use of Mn:NIR-QD for *in vivo* mapping of SLN, the left paw of a mouse was subcutaneously injected with Mn:NIR-QD in 5 μL of buffer. As the phospholipid encapsulated Mn:NIR-QD drained to the lymph node, a robust NIR signal was obtained near the left armpit up to 45 minutes post-injection. As shown in Fig. 6(b), the lymph node was initially invisible in the "bright field" mode. After applying a suitable set of filters (excitation: 661nm, emission: 700 nm long pass, integration time: 1500ms), the lymph node, which locates under the tissue, can be easily distinguished from the other tissue. Precise removal of infected lymph node can be facilitated by Mn:NIR-QDs to impede the spread of cancer.

2.4. Histological studies

In addition to the *in vivo* applications of Mn:NIR-QD, toxicity is a critical issue that needs to be addressed [20]. For safe utilization of Mn:NIR-QD, especially for these heavy-metal containing materials, understanding the interactions between QDs and biological samples is crucial. As demonstrated by Ye, Yong et. al., no toxic sign was found after systemic injection of phopholipid-micelle-encapsulated Cd-based QDs into the non-human primate rhesus macaques [19]. It implies that with good surface passivation and protection, even "high risk" materials can be safely handled and used in clinical. To access the *in vivo* toxicity of Mn:NIR-QD, histological analysis was performed on the tissues obtained from the major organs such as liver, spleen, kidney, lung, and heart to investigate for any sign of acute toxicity. Tissues were harvested at 3 weeks post injection of Mn:NIR-QD (25mg/kg) and processed for pathology evaluation. No abnormal behavior in eating, drinking, exploration or physical features were observed during this period of time. Then tissue sections were carefully analyzed by a pathologist for checking tissue toxicity. From these studies, no signs of toxicity were observed in the tissues from the animals receiving the QDs, when compared to the control animals receiving only buffer solution (Fig. 7). The results strongly suggest that the Mn:NIR-QD is nontoxic *in vivo* at this dosage.

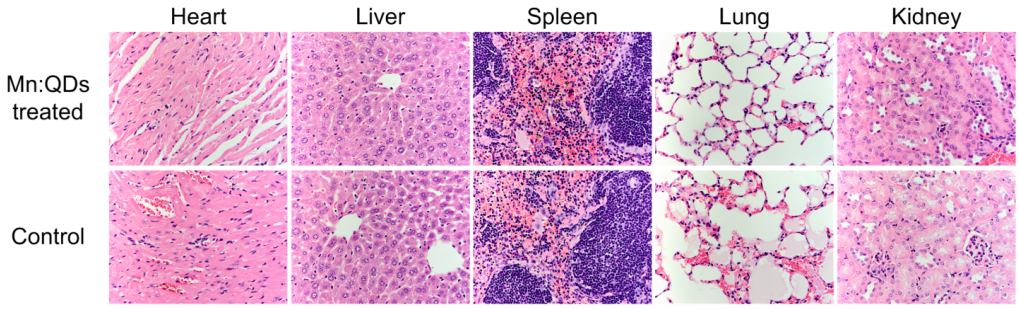

Fig. 7. Histological studies (Objective: 40x) on the major organs of the Mn:NIR-QD injected mice after 3 weeks. No damages of tissues have been found.

3. Conclusion

A hybrid approach was employed to synthesized a bimodal nanoprobe, Mn:NIR-QD. Mn-doped CdHgTe was firstly synthesized in aqueous phase followed by a phase transfer and ZnS coating. Phospholipid coated Mn:NIR-QDs exhibited hydrodynamic diameter of ~120nm, bio-functionalities, bimodal imaging contrast (optical and MR) and minimal toxicity. *In vitro* cellular uptake, tumor targeting and SLN mapping were successfully demonstrated. The integration of magnetic and optical imaging modality into one system provides a versatile platform that may be beneficial to a wide range of nanomedicine

Optics EXPRESS

applications. This work presented a facile method to prepare one of the multimodal candidates.

Funding

The Hong Kong Polytechnic University (Project Grants: 1-ZE3A and 4-BCCL); National Natural Science Foundation of China (NSFC) (61405169).